Available online at www.sciencedirect.com
ScienceDirect
Acta Materialia 57 (2009) 1132–1146
Acta MATERIALIA
www.elsevier.com/locate/actamat

Evolution of initial grain boundaries and shear bands in Cu bicrystals during one-pass equal-channel angular pressing

W.Z. Han, H.J. Yang, X.H. An, R.Q. Yang, S.X. Li, S.D. Wu *, Z.F. Zhang *

Shenyang National Laboratory for Materials Science, Institute of Metal Research, Chinese Academy of Sciences, Shenyang 110016, China

Received 25 September 2008; received in revised form 29 October 2008; accepted 1 November 2008
Available online 24 November 2008

Abstract

The evolution of grain boundaries (GBs) and shear bands in Cu bicrystals during one-pass equal-channel angular pressing (ECAP) was systematically investigated by various techniques. Four Cu bicrystals were designed to make GBs with angles of 0°, 45°, 90° and 135° with respect to the intersection plane (IP) of the ECAP die. After ECAP, the shear bands and the GB orientations in the four bicrystals displayed distinct behaviors due to the difference in the initial GB directions and the special crystallographic orientation of the component grains. Based on the experimental results, it is suggested that the initial GBs have a remarkable influence on the shear deformation behaviors of the adjacent regions, and the deformation regions far from the GBs are mainly controlled by the crystallographic orientations. The present investigations further demonstrate that shear deformation along the normal of the IP plays an important role in the deformation of Cu bicrystals.

Keywords: Cu bicrystals; Equal-channel angular pressing (ECAP); Grain boundary (GB); Shear bands

1. Introduction

For metals and alloys, the primary role of grain boundaries (GBs) is thought to be that of obstacles to dislocation motion, and the widely referenced Hall–Petch relation [1,2] predicts that decreasing the average grain size, effectively increasing the fraction of GBs, results in increased strength [1–5]. It is well known that there are several severe plastic deformation (SPD) methods to refine the grain size or increase the volume fraction of GBs in metallic crystalline materials, e.g. equal-channel angular pressing (ECAP), high-pressure torsion (HTP) and surface mechanical attrition treatment (SMAT) [6–10]. ECAP, as one of the major SPD methods, has been widely used to fabricate ultrafine-grained materials for two decades [6,7]. The mechanism of grain refinement via ECAP has been extensively investigated in numerous materials, including both polycrystals and single crystals [11–23]. However, the investigations using polycrystals cannot clearly discern the individual influences of numerous GBs and the different orientations of the component grains on the grain refinement mechanism. Therefore, the use of various kinds of single crystals provides a unique opportunity to obtain a direct evaluation to reveal the effect of crystallographic orientation on grain refinement [11–15]. However, studies using single crystals also have some obvious limitations. For example, it is not clear what the roles of the initial high-angle GBs (HAGBs) are during the process of ECAP because there are no GBs in single crystals.

In order to get a better understanding on the effect of both GB and crystallographic orientation on grain refinement, bicrystals with one flat HAGB plane are the ideal model materials. In the past decade, bicrystals have been widely employed as model materials to reveal the GB effects under monotonic and cyclic loading conditions. Winning et al. [24,25], Cahn et al. [26,27], Molodov et al. [28] and Zhang and Wang [29,30], have employed bicrystals to study the GB migration process and the GB fatigue

* Corresponding authors.
E-mail addresses: shdwu@imr.ac.cn (S.D. Wu), zhfzhang@imr.ac.cn (Z.F. Zhang).

1359-6454/$34.00 © 2008 Acta Materialia Inc. Published by Elsevier Ltd. All rights reserved.
doi:10.1016/j.actamat.2008.11.001

cracking mechanisms. Zaefferer et al. [31] and Kuo et al. [32,33] have investigated the interaction of GBs with shear deformation in bicrystals under both channel-die compression and a simple shear test conditions. They found that the deformation behavior of GBs is a function of the GB character, and the misorientation gradient is often formed in the vicinity of the GB. Paul et al. [34] investigated the strain hardening and microstructural evolution of channel-die compressed Al bicrystals and concluded that for most grain pair combinations of bicrystals the individual grain orientations played a dominant role in development of deformation substructures. However, to the authors' knowledge, there are no reports about the investigation on the microstructural evolution of bicrystals during ECAP to reveal GB effects.

It is well known that ECAP can impose very special shear deformation on the pressed metal billets, which is quite different from that in other SPD methods. For example, the large shear deformation is always considered to occur along the intersection plane (IP) between the entrance and exit channels, and the IP seems to be the shear deformation plane [35,36]. Recently, we have conducted some experiments using Al and Cu single crystals and the corresponding experimental results indicate that, in addition to the shear deformation along the IP, the shear deformation along the normal to the IP also played an important role in the plastic deformation of Al and Cu single crystals [15,37,38]. In recent papers Starink et al. [39,40] also suggested a second shear plane when modeling the texture evolution of Al alloys during ECAP. The definition of the second shear plane by Starink et al. [39,40] is just the shear deformation plane along the normal of the IP, which is very consistent with our previous ideas [15]. In order to further investigate the shear deformation mechanisms during ECAP, it is necessary to select bicrystals as model materials because the GBs in the bicrystals can be easily traced during plastic deformation. According to the deformation and evolution of the GBs in the designed bicrystals, one can judge the shear deformation mode of ECAP in detail.

In the present work, we employed four Cu bicrystals with different GB angles with respect to the IP. The interaction mechanism between the shear deformation imposed by the ECAP die and the GBs of Cu bicrystals were investigated by various techniques in order to study two issues: (1) What is the role of the initial HAGBs in grain refinement mechanisms during ECAP? (2) What is the relation between the evolution of the GBs and shear bands in those Cu bicrystals during the shear deformation mode of ECAP.

2. Materials and methods

2.1. Experimental design

The present experiments were conducted using bicrystal of high-purity oxygen-free high-conductivity Cu (99.999%) grown by the Bridgman method in a horizontal furnace [29,30]. The initial crystallographic orientations of the bicrystals were determined using the electron backscatter diffraction (EBSD) method. In order to investigate the evolution of GBs in an identical bicrystal and the interaction mechanism between shear deformation and GBs during ECAP, the initial position of the GBs in the bicrystals was designed according to the geometrical character of the ECAP die. Fig. 1 is the schematic illustration of the ECAP die and the corresponding GB locations in the four Cu bicrystals. The angles between the GBs in the four bicrystals and the extrusion direction (ED) of the ECAP die are 0°, 45°, 90° and 135°; hence the four bicrystals were named as A-GB-0°, B-GB-45°, C-GB-90° and D-GB-135°, respectively.

2.2. Preparation of Cu bicrystals and processing by ECAP

Samples of four Cu bicrystals with dimensions of about $8 \times 8 \times 40\ mm^3$ were cut according to the design from an identical bulk Cu bicrystal. The methods of cutting these Cu bicrystals are schematically illustrated in Fig. 2a. Bicrystals B-GB-45° and D-GB-135° were cut with the same format at the first stage, as shown in Fig. 2a. However, the specimen of bicrystal D-GB-135° was rotated along its insert direction (ID) for 180° before the ECAP processing, and then its GB had the designed GB location, as shown in Fig. 1. The initial {1 1 1} pole figure of the bicrystal in the vicinity of the GB is shown in Fig. 2b; Fig. 2c is the corresponding EBSD image. It can be found that one of the (1 1 1) planes of the component grains in the bicrystals is approximately parallel to the GB plane, as illustrated in Fig. 2c. The pictures of four specially designed Cu bicrystals are shown in Fig. 2d. Then these

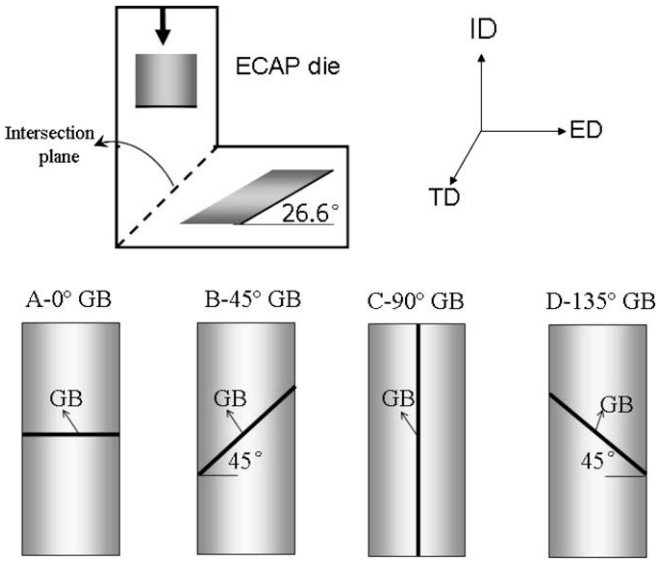

Fig. 1. Schematic illustration of the ECAP coordinates and the current experimental design (ID, insert direction; TD, transverse direction; ED, extrusion direction).

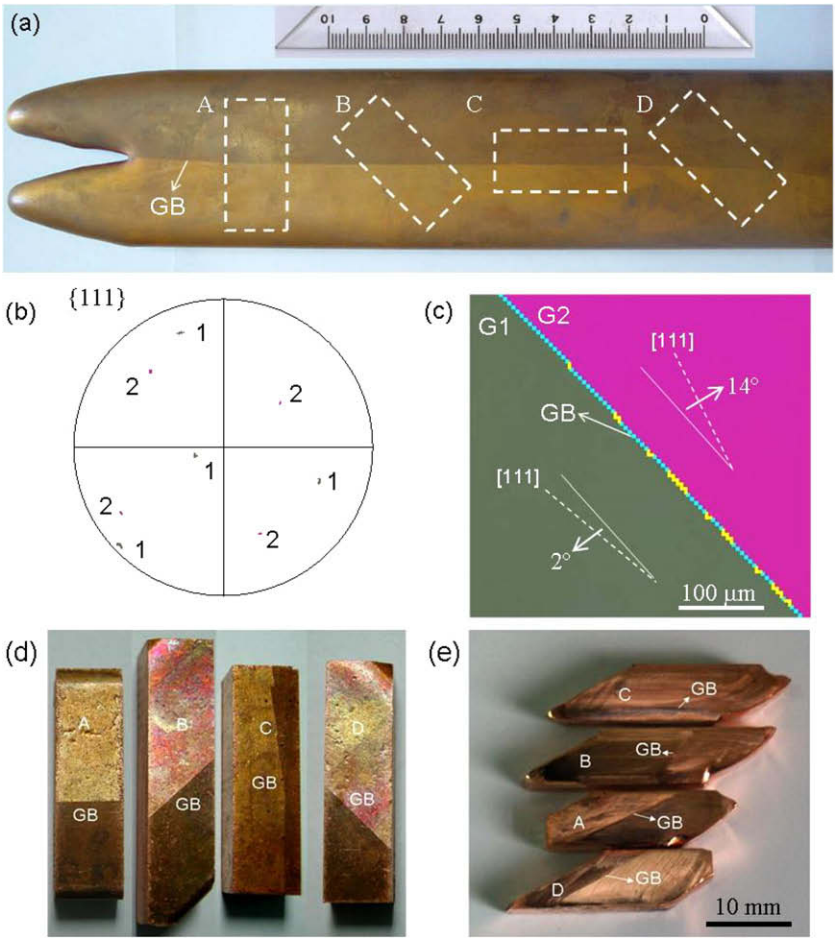

Fig. 2. (a) Schematic illustration of the preparation of Cu bicrystals; (b and c) the initial {111} pole figure of the Cu bicrystal and the corresponding EBSD image; (d) a picture of these Cu bicrystals before ECAP; (e) pictures of the four deformed Cu bicrystals.

Cu bicrystals were extruded for only one pass through a right-angle ECAP die at room temperature with an extrusion rate of 5 mm min^{-1} and lubrication of MoS_2. After ECAP, the shapes of these Cu bicrystals were significantly changed and the GBs had different angles with respect to the ED, as shown in Fig. 2e.

2.3. Microstructural characterization

After ECAP, the microstructural characterizations were performed by scanning electron microscopy (SEM; Cambridge S-360 and LEO SUPRA 35-FEG-SEM). The samples for SEM and EBSD experiments were then mechanically ground using abrasive paper and finally electropolished in a solution of alcohol and phosphoric acid. The EBSD experiments were conducted on a LEO SUPRA 35-FEG-SEM with a step size of 3 μm and the image area was set at 700×700 μm^2. In order to further observe the microstructures in the vicinity of the GBs, the polished samples were then etched and scanned by SEM. In our experimental observations, great attention was paid to the evolutions of GBs, shear bands as well as slip bands.

3. Results

3.1. Bicrystal A-GB-0°

Fig. 3 shows the SEM electron channeling contrast (SEM-ECC) images on the ID–ED plane of the bicrystal A-GB-0° in the vicinity of the GB after one pass of ECAP. It can be seen that the GB in the bicrystal A-GB-0° has an angle of ~27° with respect to the ED, as indicated in Fig. 3a. Compared with the initial GB, it has been rotated ~27° in the anticlockwise direction. The total length of the GB also was elongated and can be calculated according to the angle between the elongated GB and the ED of the ECAP die. The direction of the GB in the bicrystal A-GB-0° is similar to the shear flow lines formed in polycrystalline metals [41–48], which also make an angle of ~27° with respect to ED and can be understood in terms of material flow during ECAP [41–48]. Different directions of deformation bands were formed in order to coordinate the plastic deformation at the GB, as demonstrated in Fig. 3a and b. Some part of the GB in the bicrystal A-GB-0° can be clearly discerned, but some other parts become indistinct, forming a banding structure with a

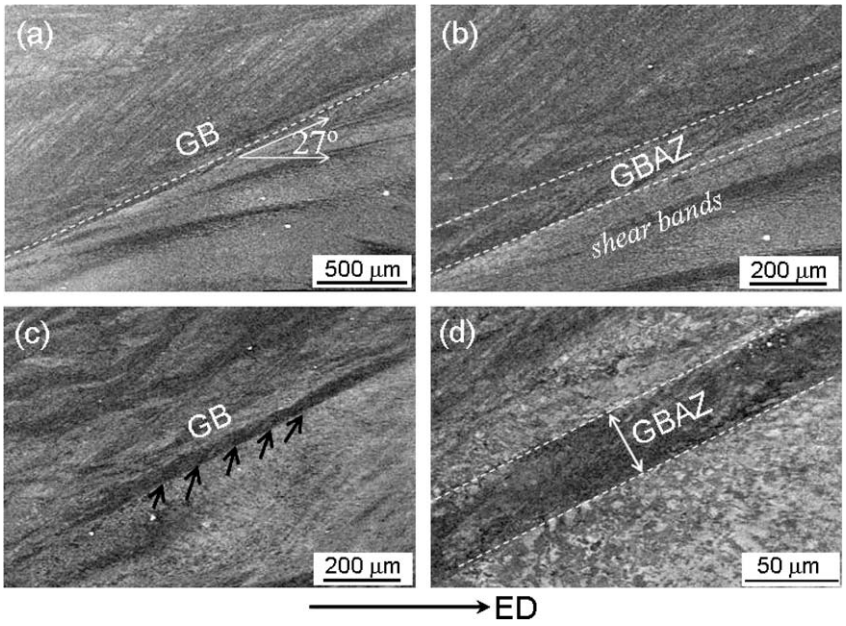

Fig. 3. Typical SEM-ECC images of bicrystal A-GB-0° on the ID–ED plane after one pass of ECAP: (a) low-magnification observation; (b)–(d) higher-magnification images.

width of ~40 μm aligned along the direction of GB, as shown in Fig. 3c and d. The formation of the banding structures must be induced by the effect of the GB. Hereafter, this kind of special deformation region induced by GB will refer to as the GB-affected zone (GBAZ).

Fig. 4 shows an SEM image of the etched bicrystal A-GB-0° after one pass of ECAP. It can be seen that the GB in the deformed bicrystal still keeps straight although it has undergone SPD, as shown in Fig. 4a–d. Profuse shear bands can be clearly observed in the vicinity of the GB, as marked in Fig. 4a and b. It should be pointed out that those shear bands did not stop at the GB, but persisted for a certain distance, as indicated in Fig. 4b. At a higher magnification, some slip traces can be found, as marked in Fig. 4d. Fig. 5 shows the EBSD images. It can be seen that the GB in the bicrystal A-GB-0° is marked by the yellow lines in the middle of Fig. 5a. The newly formed deformation structure in the bicrystal A-GB-0° has a relatively low misorientation angle (<15°), as illustrated in Fig. 5b, which is consistent with the investigations using single crys-

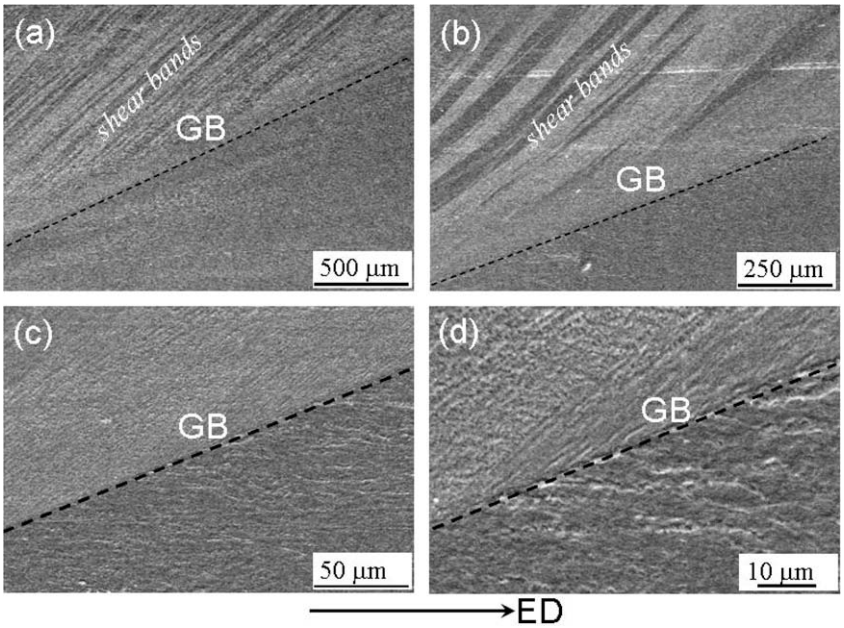

Fig. 4. SEM images of the etched bicrystal A-GB-0° on the ID–ED plane after one pass of ECAP: (a) low-magnification observation; (b)–(d) high-magnification images.

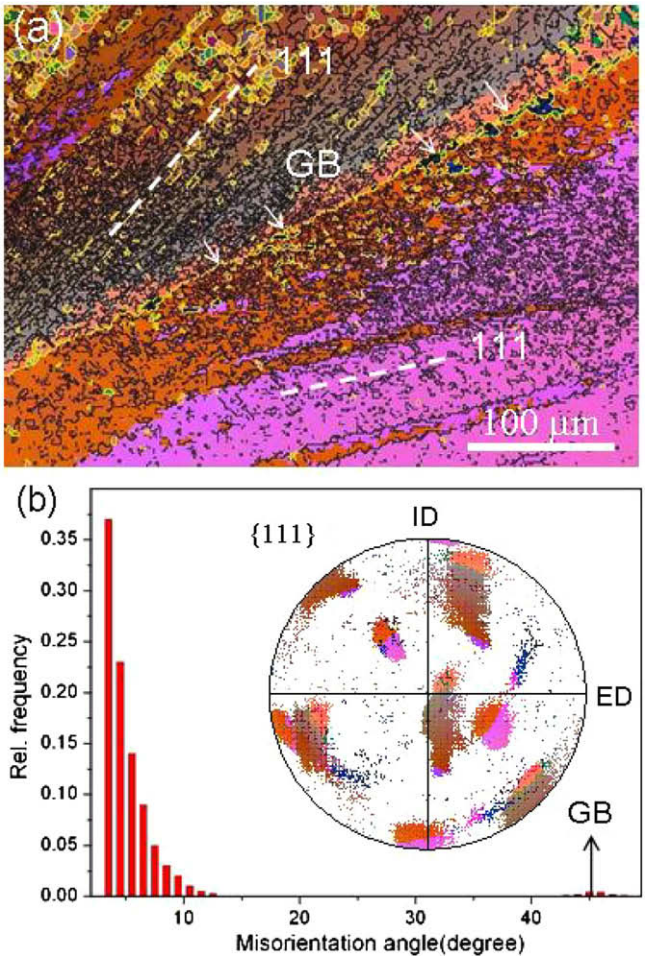

Fig. 5. The EBSD image and orientation information of the deformed bicrystal A-GB-0° on the ID–ED plane: (a) EBSD image; (b) GB misorientation distribution and the {111} pole figure.

tals [11–15]. The insert in Fig. 5b is the {111} pole figure of the deformed bicrystal A-GB-0°; it can be seen that those banding structures were formed only along a (111) plane in each component grain, as marked by the white dashed lines in Fig. 5a.

3.2. Bicrystal B-GB-45°

Fig. 6 shows the SEM-ECC images on the ID–ED plane of the bicrystal B-GB-45°. The GB of the bicrystal B-GB-45° makes an angle of ~53° with respected to the ED, as labeled in Fig. 6a. Although it has been rotated ~8° in the anticlockwise direction compared with the initial GB, the length of the deformed GB in the bicrystal B-GB-45° remains unchanged. Some shear bands were formed along similar directions in the two component grains of bicrystal B-GB-45°, as shown in Fig. 6a. In some parts, the shear bands have penetrated the initial HAGB, as demonstrated in Fig. 6b–d. Due to the intensive interactions between the shear bands and the GB, the propagation direction and the width of the shear band have changed greatly, as shown in Fig. 6b and c. When a shear band penetrated the GB, a deformation-induced step was left at the GB, as indicated by the white circle in Fig. 6d.

Fig. 7 shows another typical morphology formed in the bicrystal B-GB-45°. In this part, the GB cannot keep straight after ECAP, and appears in a wavy shape, as shown in Fig. 7a–d. Some shear bands were also formed beside the GB, as observed in Fig. 6; however, those shear bands did not penetrate the GB, while still maintaining a certain distance with respect to the GB, as observed in Fig. 7a and b. It can be found that a GBAZ with a width of about 300 μm was formed at the left side of the GB. The shear bands in the left grain stop at the boundary of GBAZ, while the shear bands in the right grain only started at the edge of the GB, as demonstrated in Fig. 7b and c. The GBAZ appears in a different contrast and its microstructures are highly jumbled and significantly different from the region far from the GB, as shown in Fig. 7c and d. The formation of the GBAZ and the curvature of the GB must be induced by the deformation incompatibility between the left and the right component grains.

Figs. 8 and 9 present SEM images of the etched bicrystal B-GB-45° after one pass of ECAP. The GB in the deformed bicrystal becomes banded due to the strong interaction between the shear bands and the GB. Clear shear bands can be observed in the etched specimen, as marked by the dashed lines in Figs. 8 and 9. Obviously, one shear band corresponds to one curvature at the region of the GB in the bicrystal B-GB-45°. Therefore the kinking deformation of the GB in the bicrystal B-GB-45° was induced by the strong shear deformation imposed by the ECAP die. Fig. 10a presents the EBSD image of the bicrystal B-GB-45° in the vicinity of the GB. It can be seen that a step was formed due to the intensive interaction between shear bands and the GB. The yellow line in the middle of Fig. 10a indicates the deformed GB. Obviously, the GB has been significantly twisted during extrusion. After ECAP, the orientation of the bicrystal B-GB−45° has been significantly scattered. Most of the GB misorientation angles are less than 15°, although some misorientation angles are larger than 15°. From the corresponding {111} pole figure in Fig. 10b, it can be deduced that the shear bands in the bicrystal B-GB-45° did not propagate along the (111) plane. These experimental results demonstrate that the bicrystal B-GB-45° has undergone more intensive plastic deformation than the bicrystal A-GB-0°.

3.3. Bicrystal C-GB-90°

Fig. 11 shows the SEM-ECC images on the ID–ED plane of the bicrystal C-GB-90° near the region of the GB. Its GB is parallel to ED and has been rotated ~90° in the anticlockwise direction during ECAP, as shown in Fig. 11a–d. The length of the deformed GB remains unchanged compared with the initial state, which is similar to that in the bicrystal B-GB-45°. Further observations around the GB indicate that the banding structures formed in the bicrystal C-GB-90° still keep a certain distance from

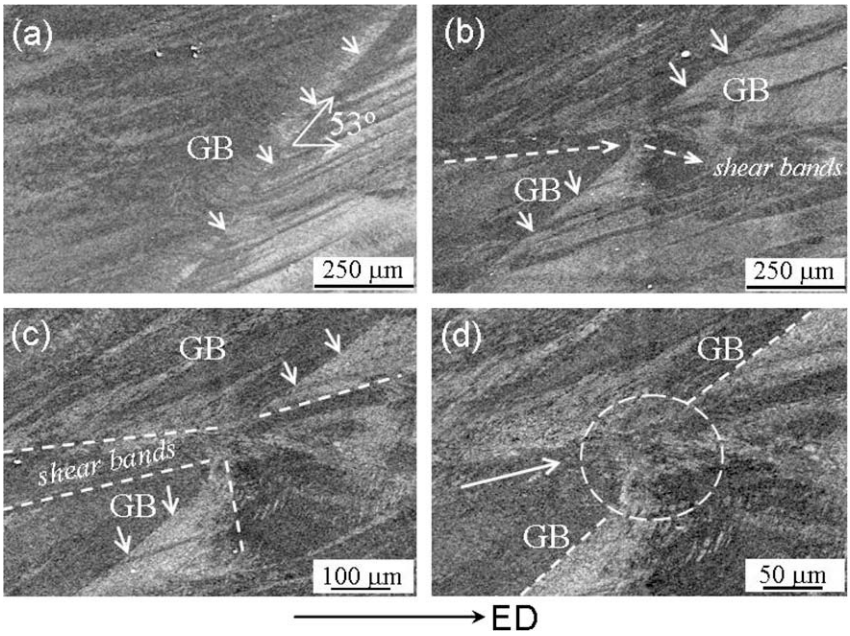

Fig. 6. Typical SEM-ECC images of the bicrystal B-GB-45° on the ID–ED plane: (a) low-magnification observation; (b)–(d) high-magnification images.

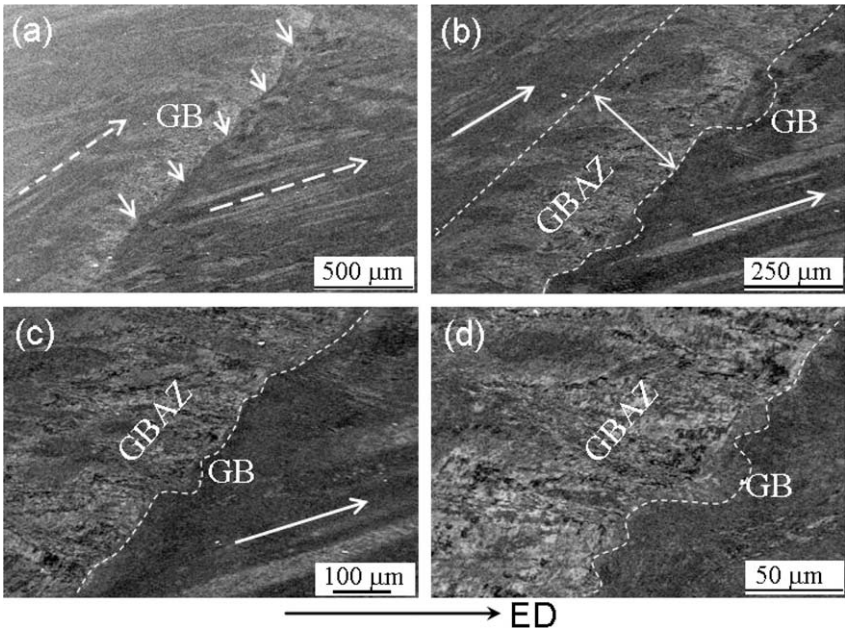

Fig. 7. Typical SEM-ECC images of the bicrystal B-GB-45° on the ID–ED plane: (a) low-magnification observation; (b)–(d) high-magnification images.

the GB, rather than penetrating it, which is different from the observations in the bicrystal B-GB-45°, as displayed in Fig. 11a–c. The magnified images at the region of the GB shown in Fig. 11c and d demonstrate that the GB of the bicrystal C-GB-90° remains straight although it has undergone SPD.

Fig. 12 shows the SEM image of the etched bicrystal C-GB-90°. When observed at low magnification, the GB in the bicrystal C-GB-90° remains straight. At the part above the GB, a few shear bands can also be found, as indicated by the dashed line in Fig. 12a. However, at a higher magnification, a series of small shear band traces can be observed at the GB, as shown in Fig. 12b–d. Those small shear bands form an angle of ~45° with respect to the GB. Due to the shear deformation along the 45° direction, the GB in bicrystal C-GB-90° has been twisted and forms a small step, as marked in Fig. 12d. Compared with that formed in the bicrystal B-GB-45°, the steps in the bicrystal C-GB-90° are very small. SEM observation of the etched sample demonstrates that the bicrystal C-GB-90° has undergone a shear deformation along the 45° direction of the GB. The corresponding EBSD image and misorienta-

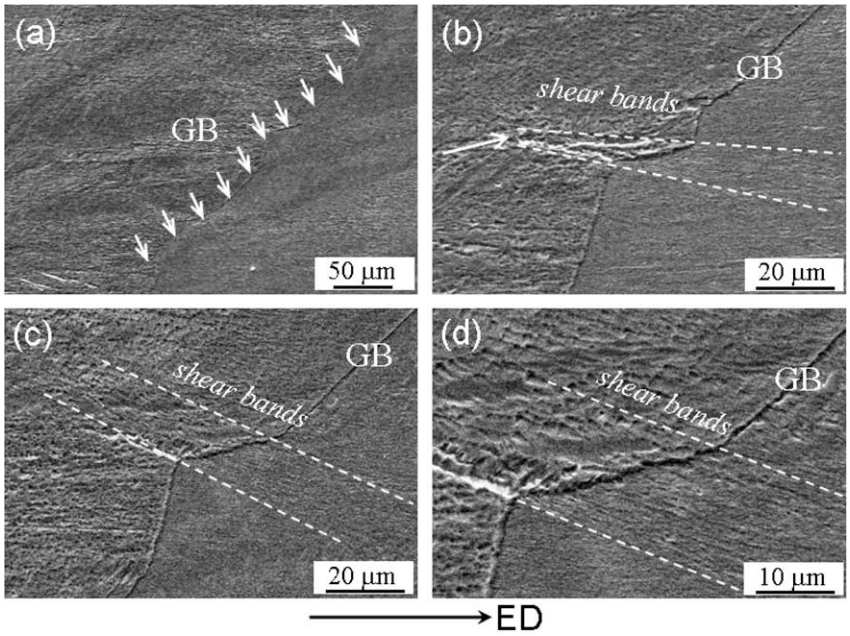

Fig. 8. SEM images of the etched bicrystal B-GB-45° on the ID–ED plane: (a) low-magnification observation; (b)–(d) high-magnification images.

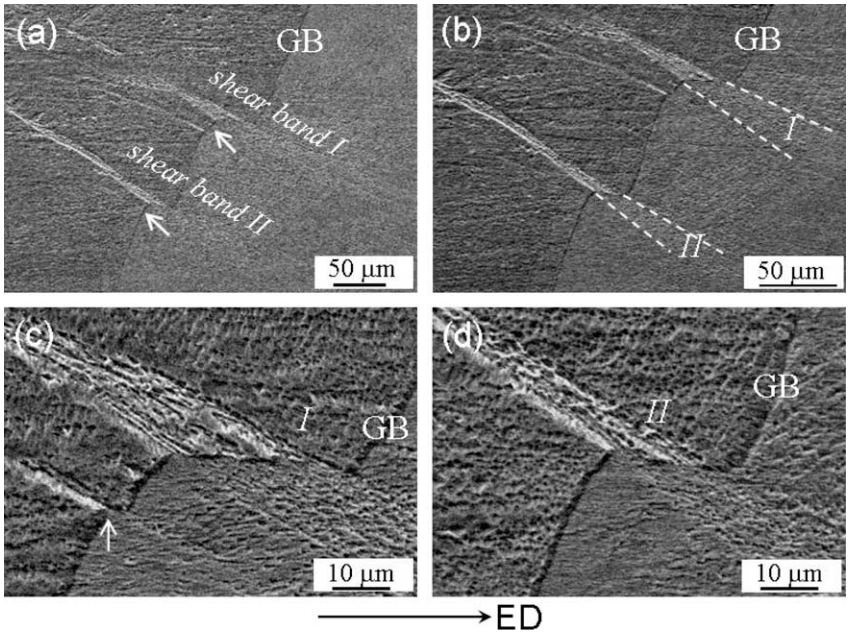

Fig. 9. SEM images of the etched bicrystal B-GB-45° on the ID–ED plane: (a) low-magnification observation; (b)–(d) high-magnification images.

tion distribution of the bicrystal C-GB-90° are presented in Fig. 13. The orientation scatter shown in Fig. 13b is relatively small compared with the bicrystal B-GB-45°, indicating that the bicrystal C-GB-90° has undergone a relatively homogeneous deformation. Most of the misorientation angles are less than 15°, which is similar to the results of the bicrystal A-GB-0°. The corresponding {1 1 1} pole figure in Fig. 13b indicates that the banding structures in the lower grain were formed along a (1 1 1) plane, while the shear bands in upper component grain did not propagate along a (1 1 1) plane.

3.4. Bicrystal D-GB-135°

Fig. 14 shows the SEM-ECC images on the ID–ED plane of the bicrystal D-GB-135°. The GB of the bicrystal D-GB-135° makes an angle of ~30° with respect to the ED and has been rotated ~75° in the anticlockwise direction during ECAP, as shown in Fig. 14a. The total length of the GB was also increased. Profuse shear bands were formed in the two sides of the GB in the bicrystal, as indicated by the white arrows in Fig. 14a. The propagation of these shear bands is approximately parallel to the GB. In

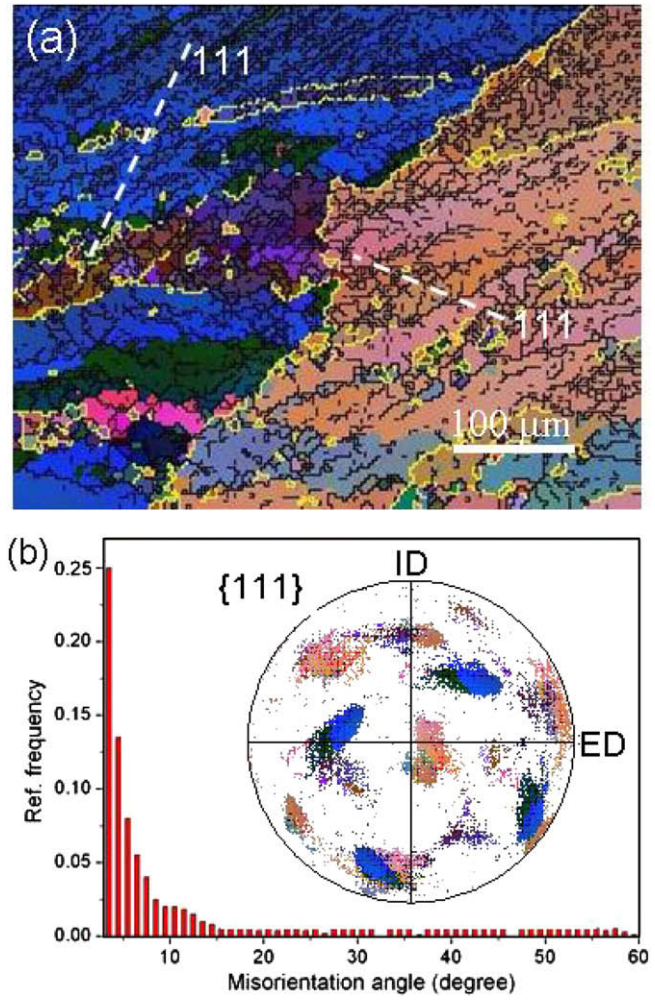

Fig. 10. The EBSD image and orientation information of the deformed bicrystal B-GB-45° on the ID–ED plane: (a) EBSD image; (b) GB misorientation distribution and the {1 1 1} pole figure.

Fig. 14b, two kinds of banding structures can be clearly discerned: one type is the same as the shear bands observed in Fig. 14a, as marked by the black arrow; another type is formed just on the two sides of the GB, as indicated by the two white arrows. The magnified observations of the second type of banding structure are shown in Fig. 14c and d. The formation of the second type of banding structure must be due to the remarkable influence of the GB on the deformation behavior of its adjacent regions. In order to accommodate the deformation around the GB, those kinds of banding structures were formed in two component grains just aligning along the GB and can also be termed a GBAZ.

Fig. 15 shows an SEM image of the etched bicrystal D-GB-135°. The GB in the deformed bicrystal D-GB-135° also remains straight although it has undergone SPD, as shown in Fig. 15a–d. Abundant shear bands can be seen in Fig. 15(a), and have a certain distance with respect to the GB, as shown by the previous observations with the SEM-ECC technique. In the vicinity of the GB, the etched bicrystal D-GB-135° has a very flat surface, indicating that those regions have undergone a relatively homogeneous deformation, which is obviously different from the region far from the GB, as shown in Fig. 15. The corresponding EBSD observation is shown in Fig. 16. Most of the formed subgrains have relatively low misorientation angles (<15°), except for the initial larger-angle GB and the deformation-induced shear banding structures, as demonstrated in Fig. 16b. The corresponding {1 1 1} pole figure in Fig. 16b indicates that the shear bands formed in the left component grain did propagate along (1 1 1) plane. Those observations clearly demonstrate that the plastic shear deformation in the bicrystal D-GB-135° indeed occurs along the direction parallel to the GB.

3.5. The influence of ECAP on the initial HAGB misorientation

In the present investigation, the four Cu bicrystal billets were cut from an identical bulk Cu bicrystal, as illustrated in Fig. 2. Therefore the initial HAGB misorientations are the same for the four bicrystals (~56°). In order to measure the misorientations of the deformed HAGB, we selected 12 random points beside the HAGB and plotted the misorientation distribution for the four Cu bicrystals, as shown in Fig. 17. It can clearly be seen that the misorientations of the four bicrystals are significantly different. The average HAGB misorientations of the bicrystal A-GB-0° are reduced by about 10° compared with the initial HAGB. The HAGB misorientations of the bicrystal B-GB-45° are scattered over a relatively wide range. Some parts are higher than the initial HAGB, but some other parts are lower than it, reflecting a relatively heterogeneous deformation for the bicrystal B-GB-45°. The HAGB misorientations of the bicrystal C-GB-90° and the bicrystal D-GB-135° are very close to the initial misorientation. However, the bicrystal C-GB-90° has a slightly lower misorientation, and the bicrystal D-GB-135° has a slightly higher misorientation. The changing of the initial HAGB misorientation of the four bicrystals during ECAP may be due to the dislocation slip or grain rotation induced by shear bands [49]. However, for the present ECAP experiment, it is hard to give a very clear explanation. Based on these experimental results, we can confirm that due to the strong interactions between shear bands and the HAGB in the bicrystal B-GB-45°, its HAGB misorientations have been scattered over a wide range.

4. Discussion

The results obtained in this investigation provide clear evidence that the evolution processes of the GBs and shear bands are strongly affected by the initial position of the GBs and the crystallographic orientations of the component grains. In the following section, we will further discuss the evolution processes of the GBs and shear bands as well as the deformation mechanisms of different Cu bicrystals during ECAP.

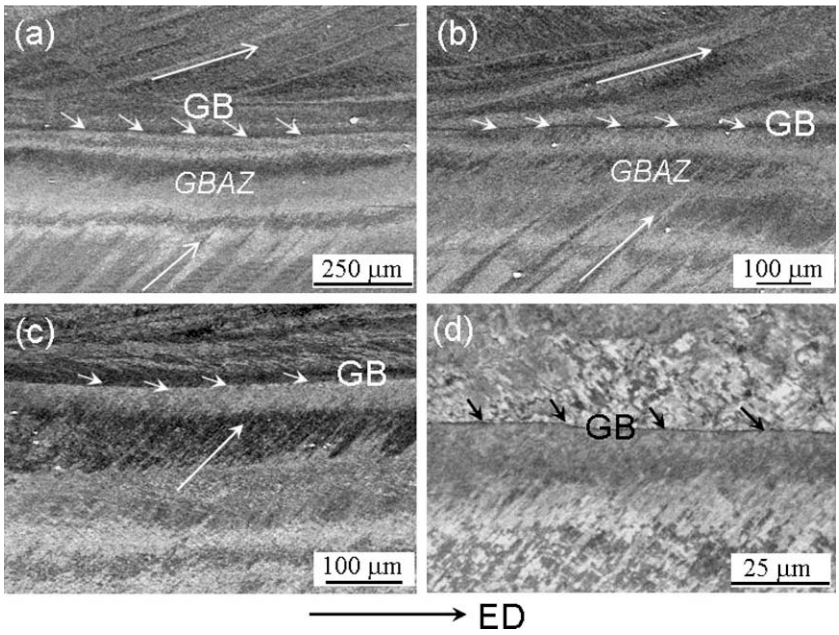

Fig. 11. The typical SEM-ECC images of the bicrystal C-GB-90° on the ID–ED plane: (a) low-magnification observation; (b)–(d) high-magnification images.

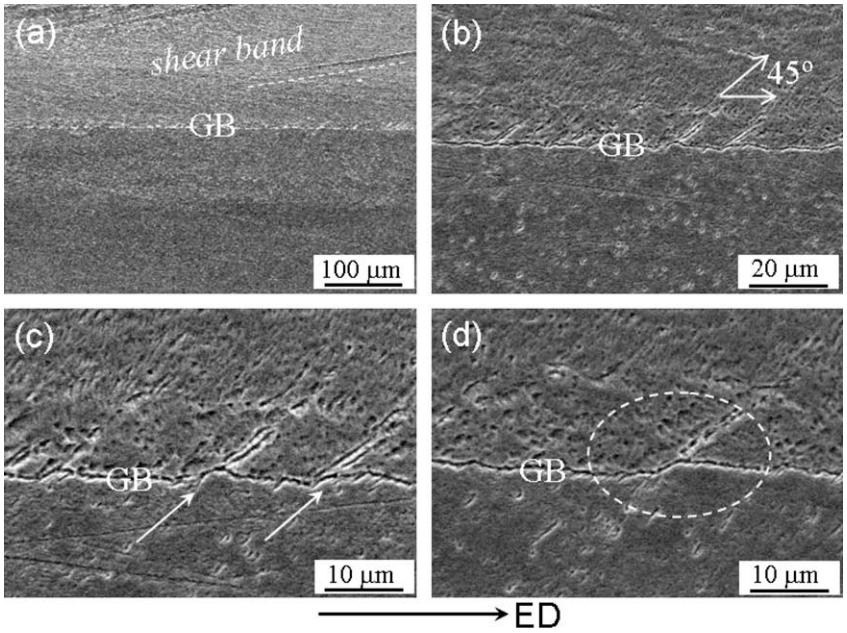

Fig. 12. SEM images of the etched bicrystal C-GB-90° on the ID–ED plane: (a) low-magnification observation; (b)–(d) high-magnification images.

4.1. Evolution of the GBs in bicrystals

It has been known that the GBs in the four Cu bicrystals have experienced different rotations and finally attain different angles with respect to ED, as listed in Table 1. The GB evolution in the bicrystal has a similar behavior as the formation process of shear flow lines in polycrystalline metals during ECAP [41–48]. According to the numerous studies on the deformation mechanism, one can figure out the general flow rules of materials during ECAP [43,44,46–48]. Considering the deformation processes of ECAP in a right-angled die, the materials may follow three rules [44,46], as illustrated in Fig. 18: (a) the material moves straight down in the vertical channel before reaching IP OO', and moves parallel to the ED in the horizontal channel after passing the IP; (b) the moving direction of the material will be changed suddenly at the IP; (c) the total moving distance of any point must be identical within the same time, i.e. $AM + MA' = BN + NB'$.

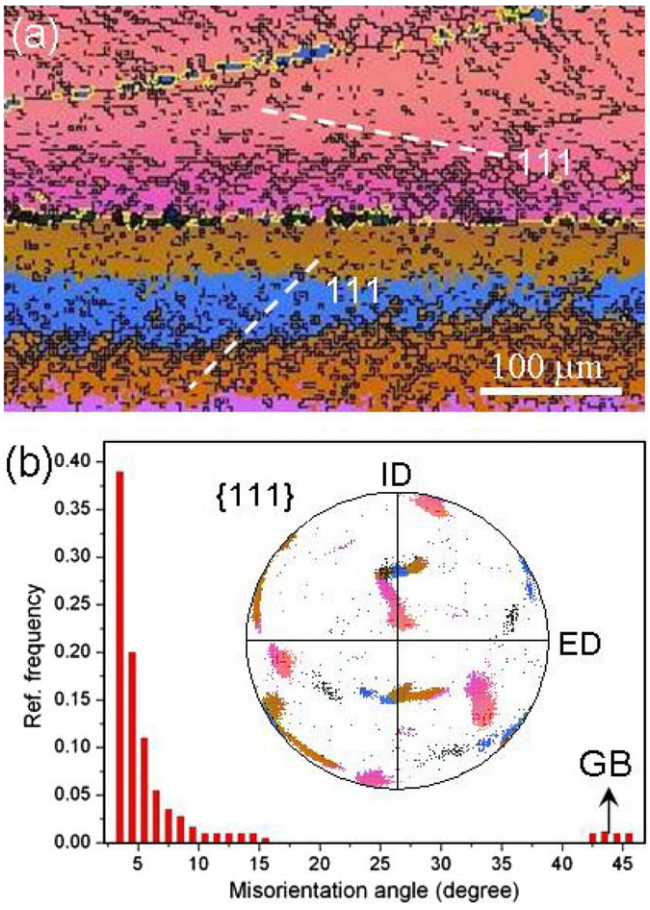

Fig. 13. EBSD image and orientation information of the deformed bicrystal C-GB-90° on the ID–ED plane: (a) EBSD image; (b) GB misorientation distribution and the {111} pole figure.

Fig. 19 shows a simple model for the deformation processes of GBs in the four bicrystals. The line AB in Fig. 19a stands for the horizontal GB in bicrystal A-GB-0°. According to the three rules above, the line AB will move straight down and remain unchanged until it reaches line A_1B_1, then the right side of line A_1B_1 in Fig. 19a firstly deforms and is directly changed into an oblique line OB_2 parallel to the final line A_0B_0, as demonstrated in Fig. 19a. Following this deformation format, the horizontal line AB will be changed into A_0B_0 piece by piece, i.e. $AB \rightarrow A_1B_1 \rightarrow A_2O_2B_2 \rightarrow \ldots \rightarrow A_0B_0$. As a result, the final line A_0B_0 compared with line AB has been stretched along the direction of line A_0B_0. Therefore the line AB will be rotated and turn into an oblique line, reaching an angle of 26.6° with respect to the ED after ECAP. This prediction is very consistent with the experimental observation as shown in Figs. 3 and 4. The schematic illustration of the evolution process of the GB in the bicrystal B-GB-45° is shown in Fig. 19b. Because the GB of the bicrystal B-GB-45° is just parallel to the IP of ECAP die, the points on line AB will reach and pass the IP at the same time according to the flow rules above [43,44,46–48]. Hence the deformation format of the GB in the bicrystal B-GB-45° can be described as $AB \rightarrow A_1B_1 \rightarrow A_2B_2 \rightarrow \ldots \rightarrow A_0B_0$. After ECAP, the GB of the bicrystal B-GB-45° should attain an angle of 45° with respect to ED and maintain the original length. This prediction is slightly different to the experimental observation above (rotated ~8°), which must be due to the strong interaction between the shear deformation imposed by the ECAP die and the GB. Besides, the effect of crystallographic orientations of the component grains also plays an important role in influ-

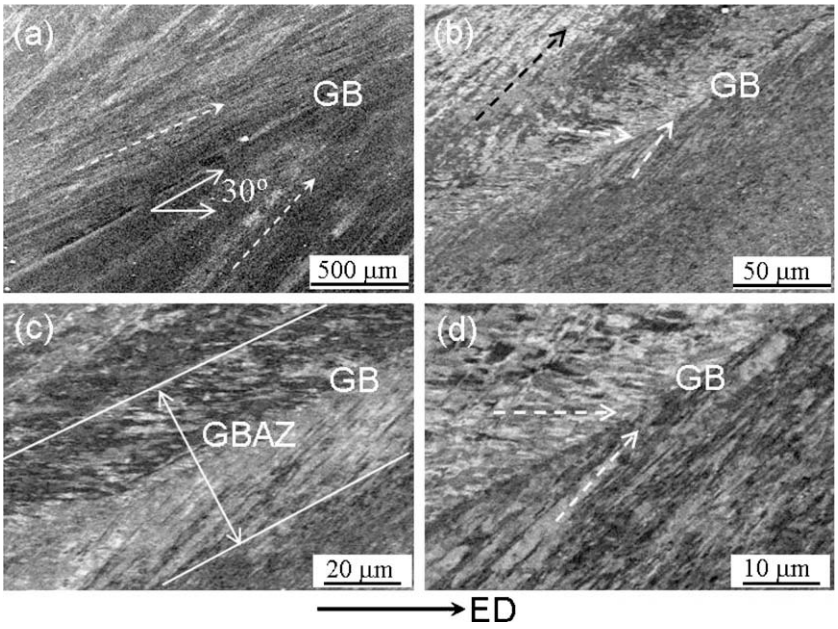

Fig. 14. Typical SEM-ECC images of the bicrystal D-GB-135° on the ID–ED plane: (a) low-magnification observation; (b)–(d) high-magnification images.

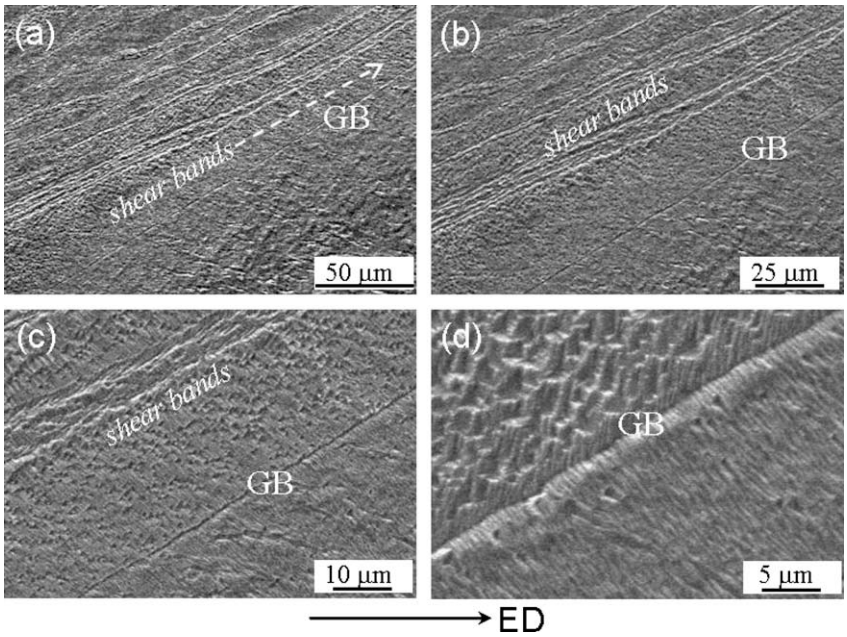

Fig. 15. SEM images of the etched bicrystal D-GB-135° on the ID–ED plane: (a) low-magnification observation; (b)–(d) high-magnification images.

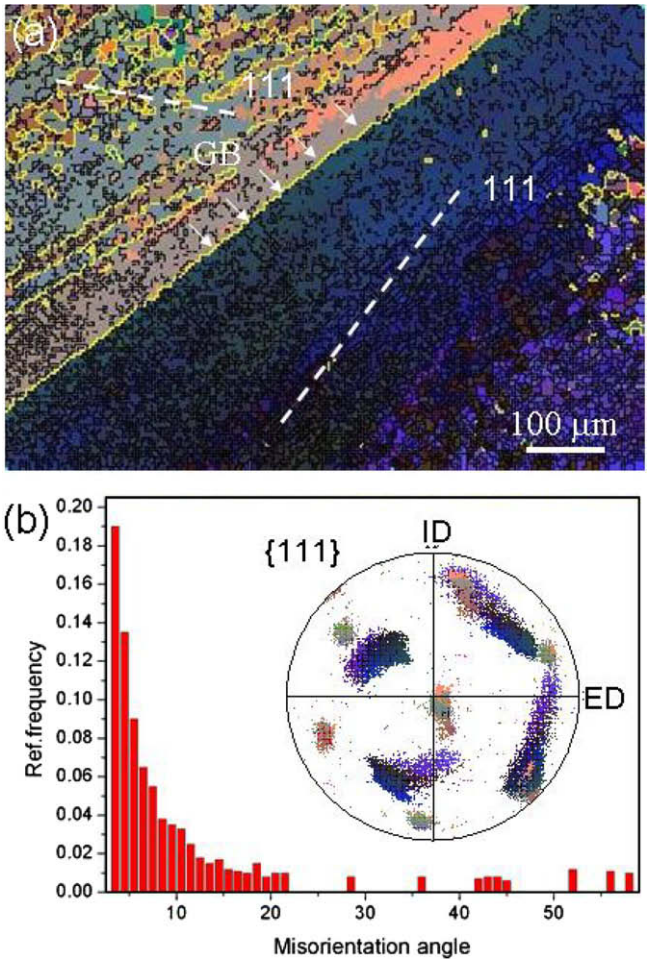

Fig. 16. EBSD image and orientation information of the deformed bicrystal D-GB-135° on the ID–ED plane: (a) EBSD image; (b) GB misorientation distribution and the {111} pole figure.

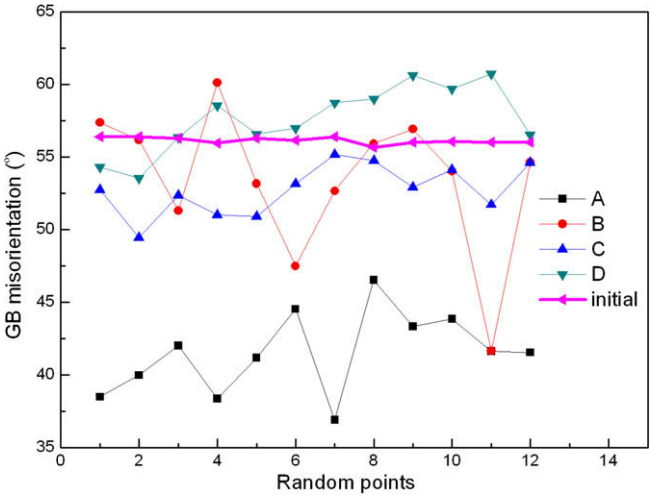

Fig. 17. The misorientation distribution of the initial HAGB and the deformed HAGB of the Cu bicrystals.

Table 1
The list of the GB parameters in the four Cu bicrystals before and after one-pass ECAP: θ_D: the initial angle between GB and ED; θ_F: the angle between GB and ED after ECAP; θ_R: the rotation angle of the GB; θ_P: the predicted angle between GB and ED according to the point view of materials flow; $\Delta\theta$: the difference between the predicted angle and the experimental observation.

Specimen No.	θ_D	θ_F	θ_R	θ_P	$\Delta\theta$	GB state
Bicrystal A-GB-0°	0°	27°	27°	27°	0°	Straight
Bicrystal B-GB-45°	45°	53°	8°	45°	8°	Curved
Bicrystal C-GB-90°	90°	0°	90°	0°	0°	Curved
Bicrystal D-GB-135°	135°	30°	75°	18.4°	11.6°	Straight

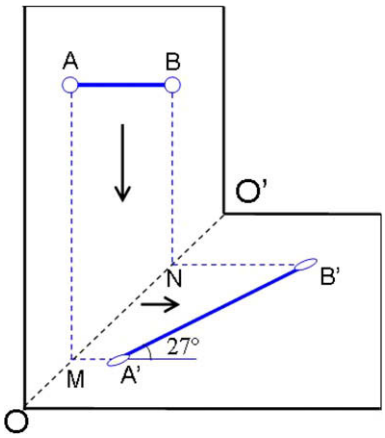

Fig. 18. Schematic illustration of the materials flow rules during ECAP.

encing the evolution of GB. The evolution processes of the GB in the bicrystal C-GB-90° are demonstrated in Fig. 19c. The initial vertical GB starts to kink little by little at the IP of the ECAP die, and finally becomes a horizontal GB without changing its length, i.e. $AB \rightarrow A_1OB_1 \rightarrow \ldots \rightarrow A_0B_0$, as illustrated in Fig. 19c. This analysis is also very consistent with the experimental observations shown in Figs. 11 and 12. The GB evolution in the bicrystal D-GB-135° has a similar feature with the bicrystal A-GB-0°, as illustrated in Fig. 19d. The evolution process can be summarized as the route: $AB \rightarrow A_1B_1 \rightarrow A_2OB_2 \ldots \rightarrow A_0B_0$. Based on the flow rules, the GB will reach an angle of ~18.4° with respect to the ED; however, the experimental observations indicate that the GB makes an angle of ~30° with respect to ED (~11° greater than that predicted), indicating that the crystallographic orientation of the grains in the bicrystal D-GB-135° also plays an important role.

4.2. Deformation mechanism of Cu bicrystals

Previous investigations have clearly demonstrated that the four bicrystals display quite different deformation behaviors when subjected to ECAP due to their different initial crystallographic orientations and the directions of their GBs. The specific deformation morphologies in the four bicrystals must be induced by the interaction between the shear deformation imposed by the ECAP die and the intrinsic slip deformation and the influence of the GBs. The schematic illustration of the deformation process of the bicrystal A-GB-0° is shown in Fig. 20. The initial (1 1 1) slip planes in each grain of the bicrystal have only a small angle with respect to the GB plane, as shown in Fig. 20a. In order to accommodate the plastic deformation of the GB, the slip systems on the (1 1 1) plane in each grain were activated during ECAP, as demonstrated in Fig. 20b. Therefore, a kind of banding structure just parallel to the (1 1 1) plane was formed in each grain after extrusion as shown in Fig. 20c. These banding structures may be induced by both the shear deformations along directions parallel and perpendicular to the IP. Due to the strengthen-

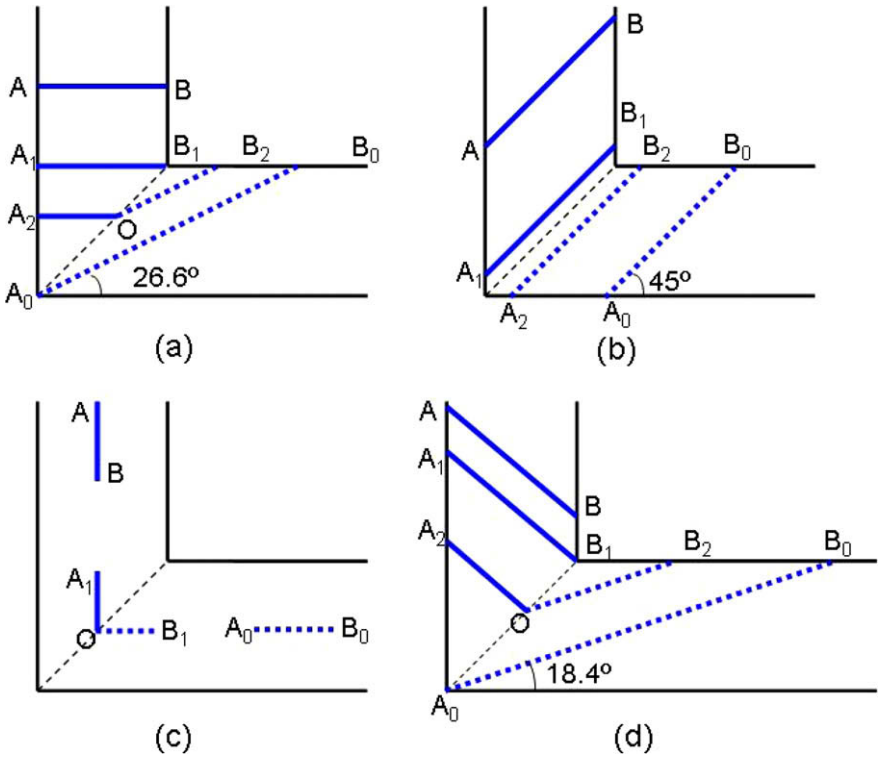

Fig. 19. Schematic illustration of the evolution process of the GBs in the four bicrystals: (a) bicrystal A-GB-0°; (b) bicrystal B-GB-45°; (c) bicrystal C-GB-90° and (d) bicrystal D-GB-135°.

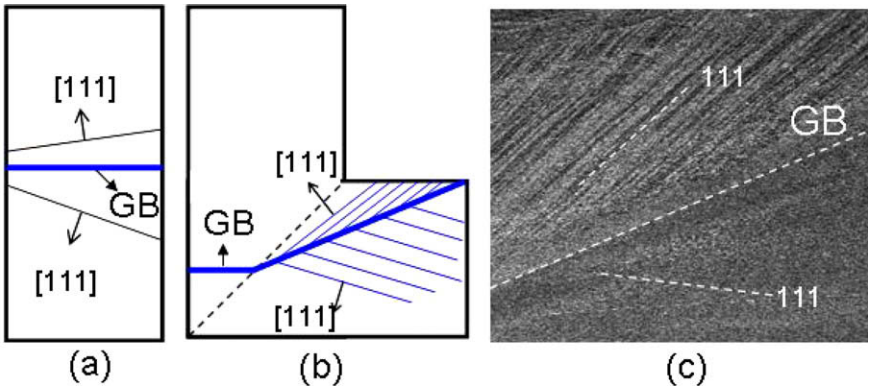

Fig. 20. Schematic illustration of the deformation process of the bicrystal A-GB-0°: (a) initial state; (b) during deformation; (c) final state.

ing effect of the GB, the region in the vicinity of the GB displays different deformation behaviors, as shown in Fig. 3.

Fig. 21 is a schematic illustration of the deformation process of the bicrystal B-GB-45°. It can be seen that its GB has been rotated a little compared with the initial GB, but was significantly bent due to the shear deformation perpendicular to the GB. Previous investigations demonstrate that in addition to the shear deformation along the IP, shear deformation perpendicular to the IP also plays an important role during ECAP [15]. Recently, Starink et al. [39,40] took the second shear plane (shear just vertical to IP) into consideration when studying the texture evolution of Al alloys during ECAP. The deformation behavior of the bicrystal B-GB-45° is closely related with the second shear stress. The initial (1 1 1) planes of the bicrystal B-GB-45° are approximately parallel to the GB plane; in other words, the (1 1 1) planes of the bicrystal B-GB-45° are parallel to the IP, as shown in Fig. 21a. Some finer slip traces parallel to the IP can also be seen in the upper component grain, showing that shear deformation along IP occurs. However, the shear deformation along the direction vertical to the IP also plays an important role during ECAP, hence a series of shear bands were formed along the direction vertical to the IP. Due to the strong interaction between shear bands and GB, the GB was severely deformed, forming deformation kinks, steps and so on, as illustrated in Fig. 21b and shown in Fig. 21c.

The schematic illustration of the deformation process in the bicrystal C-GB-90° is demonstrated in Fig. 22. The initial (1 1 1) planes of the bicrystal C-GB-90° are also approximately parallel to the GB plane. Different deformation morphologies were formed in each grain in order to accommodate the plastic deformation. On the one hand, several shear bands not propagating along the slip plane were formed in the upper grain; on the other hand, many slip bands were formed in the lower grain due to shear deformation along the 45° GB direction. Previous analysis demonstrates that the shear stress along the normal of IP plays an important role [15,37,38]. At the initial stage, profuse slip bands and shear bands were formed due to the shear deformation along the normal direction of IP. After ECAP, the GB in bicrystal C-GB-90° has been rotated about ~90°, and as a result those slip bands and shear bands will have an angle of 45° with respect to ED at the final state, as shown in Fig. 22c.

Fig. 23 is a schematic illustration of the deformation process in the bicrystal D-GB-135°. According to the initial pole figure, one can find that the (1 1 1) plane of the bicrystal D-GB-135° is also approximately parallel to the GB

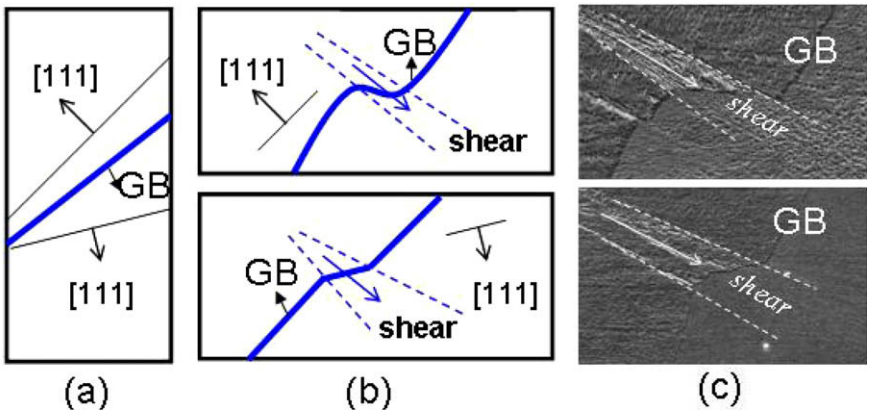

Fig. 21. Schematic illustration of the deformation process of the bicrystal B-GB-45°: (a) initial state; (b) during deformation; (c) final state.

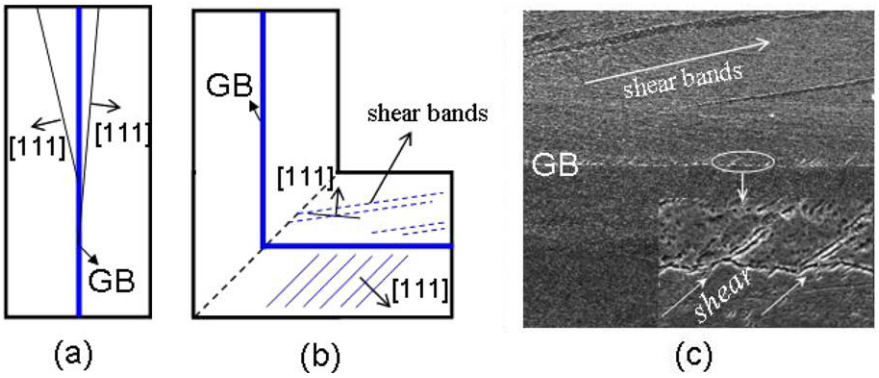

Fig. 22. Schematic illustration of the deformation process of the bicrystal C-GB-90°: (a) initial state; (b) during deformation; (c) final state.

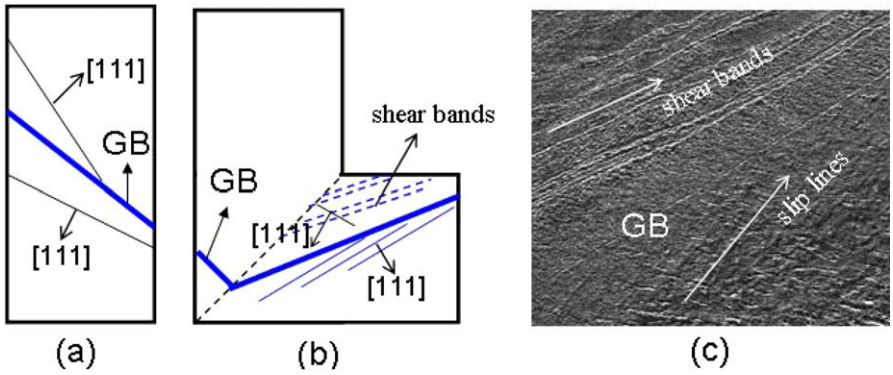

Fig. 23. Schematic illustration of the deformation process of the bicrystal D-135°: (a) initial state; (b) during deformation; (c) final state.

plane, whereas the GB of the bicrystal D-GB-135° is just perpendicular to the IP of ECAP die, as illustrated in Fig. 23a. Since one of the maximum shear stresses is along the normal direction of IP, the shear deformation occurs just along the direction of GB, and as a result many shear bands were formed along the GB, as illustrated in Fig. 23b and shown in Fig. 23c. The deformation processes of the bicrystals B-GB-45° and D-GB-135° indicate that the shear stress along the direction normal to IP plays an important role in the plastic deformation of Cu bicrystals.

5. Conclusions

Four Cu bicrystals with different initial GB directions were subjected to one pass of ECAP. The evolution of shear bands and GBs was characterized by various techniques. Based on the experimental observations and the analyses, the following conclusions can be drawn.

(1) The GBs of four Cu bicrystals have different rotations during ECAP and reach different angles with respect to ED. The GB of bicrystal C-GB-90° has the largest rigid body rotation, while the bicrystal B-GB-45° has the smallest rigid body rotation among the four bicrystals during ECAP. The evolution of the GB in bicrystals A-GB-0° and C-GB-90° can be understood based on the flow rules of materials during ECAP, while for bicrystals B-GB-45° and D-GB-135°, there exists a slight discrepancy between prediction and experimental observation, which may be due to the different crystallographic orientations of the two component grains.

(2) During the process of ECAP, the four bicrystals display quite distinct deformation behaviors due to their different initial GB directions and the specific crystallographic orientations of the component grains. The evolution process of the shear bands and the GBs in those bicrystals were analyzed according to the shear deformation mode of ECAP. Based on the experimental results and the analyses, it is suggested that shear deformations both parallel and perpendicular to IP play important roles in the ECAP process of bicrystals.

Acknowledgments

This work is supported by National Natural Science Foundation of China (NSFC) under Grant Nos. 50571102, 50890137 and 50171072. Zhang Z.F. would like to acknowledge the financial support of the "Hundred of Talents Project" of the Chinese Academy of Sciences and the National Outstanding Young Scientist Foundation under Grant No. 50625103.

References

[1] Hall EO. Proc Phys Soc B 1951;64:747.
[2] Petch NJ. J Iron Steel Inst 1953;174:25.
[3] Valiev RZ, Korznikov AV, Mulyukov RR. Mater Sci Eng A 1993;168:141.
[4] Gleiter H. Acta Mater 2000;48:1.
[5] Lu L, Shen YF, Chen XH, Lu K. Science 2004;304:422.
[6] Valiev RZ, Islamgaliev RK, Alexandrov IV. Prog Mater Sci 2000;45:103.
[7] Valiev RZ, Langdon TG. Prog Mater Sci 2006;51:881.
[8] Hansen N. Metall Mater Trans A 2001:322917.
[9] Lu K, Lu J. Mater Sci Eng A 2004;375:38.
[10] Lowe TC, Valiev RZ, editors. Investigations and application of severe plastic deformation. Dordrecht: Kluwer; 2000.
[11] Fukuda Y, Oh-ishi K, Furukawa M, Horita Z, Langdon TG. Acta Mater 2004;52:1387.
[12] Fukuda Y, Oh-ishi K, Furukawa M, Horita Z, Langdon TG. Mater Sci Eng A 2006;420:79.
[13] Miyamoto H, Erb U, Koyama T, Mimaki T, Vinogradov A, Hashimoto S. Philos Mag Lett 2004;84:235.
[14] Miyamoto H, Fushimi J, Mimaki T, Vinogradov A, Hashimoto S. Mater Sci Eng A 2005;405:221.
[15] Han WZ, Zhang ZF, Wu SD, Li SX. Acta Mater 2007;55:5889.
[16] Iwahashi Y, Horita Z, Nemoto M, Langdon TG. Acta Mater 1997;45:4711.
[17] Iwahashi Y, Horita Z, Nemoto M, Langdon TG. Acta Mater 1998;46:3317.
[18] Gholinia A, Prangnell PB, Markushev MV. Acta Mater 2000;48:1115.
[19] Dalla Torre F, Lapovok R, Sandin J, Thomson PF, Davies CHJ, Pereloma EV. Acta Mater 2004;52:4819.
[20] Xu C, Furukawa M, Horita Z, Langdon TG. Acta Mater 2003;51:6139.
[21] Shin DH, Kim I, Kim J, Park KT. Acta Mater 2001;49:1285.
[22] Stolyarov VV, Zhu YT, Alexandrv IV, Lowe TC, Valiev RZ. Mater Sci Eng A 2003;343:43.
[23] Vinogradov A, Patlan V, Suzuki Y, Kitagawa K, Kopylov VI. Acta Mater 2002;50:1639.
[24] Winning M, Gottstein G, Shvindlerman LS. Acta Mater 2001;49:211.
[25] Winning M. Acta Mater 2003;51:6465.
[26] Cahn JW, Taylor JE. Acta Mater 2004;52:4887.
[27] Cahn JW, Mishin Y, Suzuki A. Philos Mag 2006;86:3965.
[28] Molodov DA, Ivanov VA, Gottstein G. Acta Mater 2007;55:1843.
[29] Zhang ZF, Wang ZG. Acta Mater 2003;51:347.
[30] Zhang ZF, Wang ZG. Prog Mater Sci 2008;53:1025.
[31] Zaefferer S, Kuo JC, Zhao Z, Winning M, Raabe D. Acta Mater 2003;21:4719.
[32] Chen D, Kuo JC, Tung SH, Shih MH. Mater Sci Eng A 2007;454:523.
[33] Kuo JC, Chen D, Tung SH, Shih MH. J Mater Sci 2007;42:7673.
[34] Paul H, Driver JH, Wajda W. Mater Sci Eng A 2008;477:282.
[35] Segal VM. Mater Sci Eng A 1995;197:157.
[36] Segal VM. Mater Sci Eng A 2003;345:36.
[37] Han WZ, Chen GM, Li SX, Wu SD, Zhang ZF. Phys Rev Lett 2008;101:115505.
[38] Han WZ, Zhang ZF, Wu SD, Li SX. Philos Mag 2008;88:3011.
[39] Wang SC, Starink MJ, Gao N, Qiao XG, Xu C, Langdon TG. Acta Mater 2008;56:3800.
[40] Starink MJ, Wang SC, Qiao XG, Gao N, Roven HJ, Langdon TG. Mater Sci Form 2008;584–586:679.
[41] Han BQ, Lavernia EJ, Mohamed FA. Metall Mater Trans A 2003;34:71.
[42] Han WZ, Zhang ZF, Wu SD, Li SX, Wang YD. Philos Mag Lett 2006;86:435.
[43] Shan AD, Moon IG, Ko HS, Park JW. Scripta Mater 1999;41:353.
[44] Han WZ, Zhang ZF, Wu SD, Li SX. Philos Mag Lett 2007;87:735.
[45] Fukuda Y, Oh-ishi K, Horita Z, Langdon TG. Acta Mater 2002;50:1359.
[46] Han WZ, Zhang ZF, Wu SD, Li SX. Mater Sci Eng A 2008;476:224.
[47] Furukawa M, Iwahashi Y, Horita Z, Nemoto M, Langdon TG. Mater Sci Eng A 1998;257:328.
[48] Furukawa M, Horita Z, Langdon TG. Mater Sci Eng A 2002;332:97.
[49] Margulies L, Winther G, Poulsen HF. Science 2001;291:2392.